agronomy

MDPI

Article

Accurate Measurement of Frozen Soil Depth Based on I-TDR

Haoqin Qin [1], Zhiquan Mu [1], Xingyue Jia [2], Qining Kang [1], Xiaobin Li [3] and Jinghui Xu [1,*]

[1] College of Water Resources and Architectural Engineering, Northwest A&F University, Xianyang 712100, China; qhq0122@nwafu.edu.cn (H.Q.); mzq-8867@nwafu.edu.cn (Z.M.); kqn18946507421@nwafu.edu.cn (Q.K.)
[2] College of Electronic and Information Engineering, Nanjing University of Aeronautics and Astronautics, Nanjing 210016, China; xxy061ab@163.com
[3] College of Natural Resources and Environment, Northwest Agricultural and Forestry University, Xianyang 712100, China; li1996@nwafu.edu.cn
* Correspondence: xjh@nwafu.edu.cn; Tel.: +86-189-9129-9259

Abstract: In this study, a new method for determining the depth of frozen soil, Impulse Response Time Domain Reflectometry, is discussed. This method uses the principle of impedance measurement and the law of time–frequency domain convolution to convert the frequency-domain reflection signal into a time-domain signal and accurately determines the soil freezing front by measuring the difference between the impedance of frozen soil and unfrozen soil. The advantage of this method is that it solves the problems of small bandwidth, long rising edge time, and large measurement errors in the traditional TDR method to effectively improve the measurement accuracy of the soil-freezing front. Under laboratory conditions, soils of different textures (sand, loess, black soil, and red soil) were selected for experimental determination, and the results showed that compared with the traditional TDR method, the RMSE of the I-TDR method was small, and the method was applicable under different soil texture conditions, which could provide a new method for monitoring frozen soil in cold areas. In addition, the application of this method has important guiding significance for improving the efficiency of winter irrigation water, especially for guiding agricultural production, farmland irrigation, drainage engineering construction, meteorological frozen soil monitoring, and other aspects in cold and arid areas.

Keywords: soil freezing depth; time domain frequency domain transformation; I-TDR technology; impedance variation

Citation: Qin, H.; Mu, Z.; Jia, X.; Kang, Q.; Li, X.; Xu, J. Accurate Measurement of Frozen Soil Depth Based on I-TDR. *Agronomy* **2023**, *13*, 1389. https://doi.org/10.3390/agronomy13051389

Academic Editors: Xuebin Qi, Ping Li, Zhenjie Du, Zulin Zhang and Pablo Martín-Ramos

Received: 11 April 2023
Revised: 12 May 2023
Accepted: 16 May 2023
Published: 17 May 2023

1. Introduction

Seasonally frozen soil is widely distributed, and its monitoring is of great significance in engineering geology [1], climate change [2], spring flood control [3], and water-saving irrigation [4]. Monitoring soil freezing depth in a specific area can reflect climate change in that area. With the frequent increase in the La Nina phenomenon, researchers are paying increasing attention to the determination of the freezing depth of seasonally frozen soils [5]. The frozen front is the boundary between the frozen and unfrozen soil layers during the development of the frozen soil layer, and its position is dynamic during the freezing and thawing processes [6]. Taking the unidirectional freezing in the open system as an example, with the continuous decrease in the soil surface temperature, the upper frozen soil zone will gradually develop downward, and the water in the lower unfrozen soil zone will approach the cold end under the effect of the temperature gradient, the frozen front position then moves downward [7]. Monitoring the position of the freezing front during soil freezing can not only explore the law of soil water movement and improve the dynamic monitoring level of the soil freezing process, but also grasp the content of stagnant water at the top of the frozen soil area which is of great significance for improving the construction level of frozen soil areas [8], preventing secondary damage caused by frozen soil in agricultural production [9], and sensing ecological climate change [10]. At present, accurate monitoring of the depth of frozen peak surfaces is difficult.

Currently, research on frozen soil mainly focuses on the interactions between soil components when the temperature decreases [11], such as the mutual transformation between frozen and unfrozen soil caused by the phase change of ice and water in the soil under the influence of temperature [12], pressure [13], and mineral particles [14]. However, there are few studies on the depth detection of frozen soil. There are mainly theoretical and instrumental models in terms of frozen soil depth. Considering that the development of frozen soil is mainly due to the ice–water phase change of particles under the condition of water–heat coupling, the theoretical model mainly reflects the development law of frozen soil by simulating the transfer processes of water, heat, and dissolved mass during soil freezing and thawing. A representative example is the SHAW model proposed by Gerald [15]. As a one-dimensional multi-layer water–heat coupling model, it can describe the one-dimensional vertical water–heat transfer process of the soil–vegetation–atmosphere and can be used to predict the soil freezing depth [16]. However, the model requires many parameters including site, meteorological, soil water and heat data, and vegetation characteristics. It is necessary to set the initial and boundary values of the soil temperature and moisture and the geological characteristic data at the measuring point. For different soil characteristics, it is necessary to reset the parameters for calculation which is inconvenient [17].

Instrumental methods for monitoring soil freezing depth include the permafrost method [18], thermistor method [19], fiber grating method [20], remote sensing detection method [21], and ground penetrating radar method [22]. The traditional Danilin-type permafrost pre-deepens the water injection soft hose to a length mark 0.5 to 4.5 m underground. After freezing for a certain period, the position of ice in the hose can be determined according to its hardness through manual contact with the hose, which is equivalent to the number of frozen layers and the frozen depth of the underground soil. Sudisman et al. studied the influence of vertically buried pipes on the heat conduction of sand during seepage under freezing conditions based on the principle of permafrost [23]. However, this method is easily affected by the subjective judgment of operators and the bending of rubber pipes, and the experimental process is cumbersome. The thermistor method determines the freezing depth of a soil mass by measuring the position of the geothermal layer at 0 °C. Sveen et al. used the thermistor method to study the rapid thawing of frozen soil under cyclic heating [24]. This method requires excavating the soil and burying the equipment before backfilling which significantly disturbs the undisturbed soil, and the sensor is prone to deformation owing to frost heave during the soil freezing process which affects the measurement accuracy. The fiber grating method uses the refraction of an ultraviolet laser to form numerous weak reflection surfaces with the same spacing in the fiber core to reflect waves of a specific wavelength [25]. The characteristics of the reflection wavelength are related to the temperature, stress, and strain of the object to be measured [26]. The temperature change relationship of the object to be measured can be obtained by observing the wavelength change through the demodulation device. Cao et al. measured the temperature and humidity profiles of partially frozen soil using the improved fiber grating method, estimated the unfrozen water content and ice content of the soil under four different landforms using an aluminum oxide tube sensor system and frequency domain reflection technology, and demonstrated the impact of the type of upper cover on the downward migration of surface water [27]. However, this method is technically complex and the use of instruments and optical fiber devices is not convenient for field acquisition. Remote sensing detection methods primarily use satellite technology to perform large-scale and spatially continuous surface measurements [28]. However, satellite remote sensing can only measure surface reflection information, and frozen peak surfaces are mostly located deep underground. Therefore, it is usually necessary to combine satellite remote sensing data with mathematical and physical models to calculate the depth of frozen soil using physical models [29]. Zhang et al. proposed the concept of microwave radiation response depth (MRRD) and pointed out that soil temperature, soil texture, and frequency are the three main factors affecting the satellite radiation response [30]. The MRRD of frozen soil was estimated by establishing a three-parameter model to reflect the relationship between passive remote sensing signals and the soil freezing depth. The ground-penetrating radar method mostly uses antennas to transmit high-frequency pulsed electromagnetic waves to a detection target [31]. The electromagnetic waves reflected back to the ground are received by the receiving antenna. When electromagnetic waves propagate in an underground medium, they reflect when they encounter an interface with electrical differences [32]. The structure, shape, and burial depth of the underground medium are inferred based on the waveform, amplitude, intensity, and time characteristics of the electromagnetic waves received. Jadoon et al. used a horn antenna to set up a ground penetrating radar (GPR) system in farmland to monitor the freezing and thawing process of soil under natural snow conditions for nine days and described the freezing front through sensor settings [33]. However, ground-penetrating radars are expensive and not conducive to technological promotion.

Based on the principle of impedance reflection and time–frequency conversion, this study proposed a method for accurately measuring the frozen front of soil using Impulse response Time Domain Reflection (I-TDR) technology. The I-TDR technology uses a portable vector network analyzer to monitor the frozen peak surface using an innovatively designed printed circuit board (PCB) probe as the monitoring probe. The vector network analyzer has the characteristics of accurate measurement, high resolution, and minimal influence from external factors. Through I-TDR technology, a high-resolution TDR signal can be achieved, which makes the position of the soil freezing front better reflected in the waveform and has good application prospects.

2. Materials and Methods

2.1. Principles of Soil Impedance Measurement

The most important indicator for measuring a PCB transmission line is its characteristic impedance. During signal transmission, a transient current is generated between the signal line and the reference plane owing to the establishment of the electric field. If the transmission line is isotropic, there will always be a transient current I as long as the signal is transmitted. If the transient voltage of the signal is V, the transmission line will be equivalent to the resistance during the signal transmission. This equivalent resistance is called the characteristic impedance of a transmission line.

During signal transmission, the signal is reflected at nodes with discontinuous impedance if the characteristic impedance of the transmission path changes. A Vector Network Analyzer (VNA) excites the Device Under Test (DUT) by generating a continuously swept sine wave from the signal source. The time-domain impulse-response characteristics can be obtained using an inverse Fourier transform of the reflected frequency response [34]. Compared with the traditional TDR, which reflects the changes in the process of signal propagation through a step response, the impulse response focuses more on the time domain information of impedance discontinuity points in the process of signal propagation, rather than the characteristic differences between different media. The three signal response relationships are shown in Figure 1. During soil freezing front measurements, the probe was placed in a heterogeneous medium. To calculate a non-uniform transmission line, a simple algorithm can be used to calculate the input impedance [35]. The algorithm starts from the terminal of the transmission line, and the calculation process is as follows Equations (1)–(3):

$$Z_{in}(z_n) = Z_L, \tag{1}$$

$$Z_{in}(z_i) = Z_{c,i+1}\frac{Z_{in}(z_{i+1}) + Z_{c,i+1}tan(\gamma_{i+1}l_{i+1})}{Z_{c,i+1} + Z_{in}(z_{i+1})tan(\gamma_{i+1}l_{i+1})}, \tag{2}$$

$$Z_{in}(0) = Z_{c,1}\frac{Z_{in}(z_1) + Z_{c,1}tan(\gamma_1 l_1)}{Z_{c,1} + Z_{in}(z_1)tan(\gamma_1 l_1)}, \tag{3}$$

where $z_{c,i}$ and γ_i are the characteristic impedance and propagation constant of section i, respectively, $Z_{in}(z_i)$ is the input impedance of the corresponding circuit at z_i, l is the length of the transmission line, and Z_L is the load impedance at z = l (Z_L = 1 for an open end or zero for a shorted end). According to the boundary condition at Z = 0, the sampling voltage V(0) can be calculated as Equation (4):

$$V(0) = \frac{Z_{in}(0)}{Z_s + Z_{in}(0)}V_s, \tag{4}$$

where V(0) is the sampling voltage, Z_s is the measurement system source impedance (Z_s = 50), and V_S is the independent voltage source.

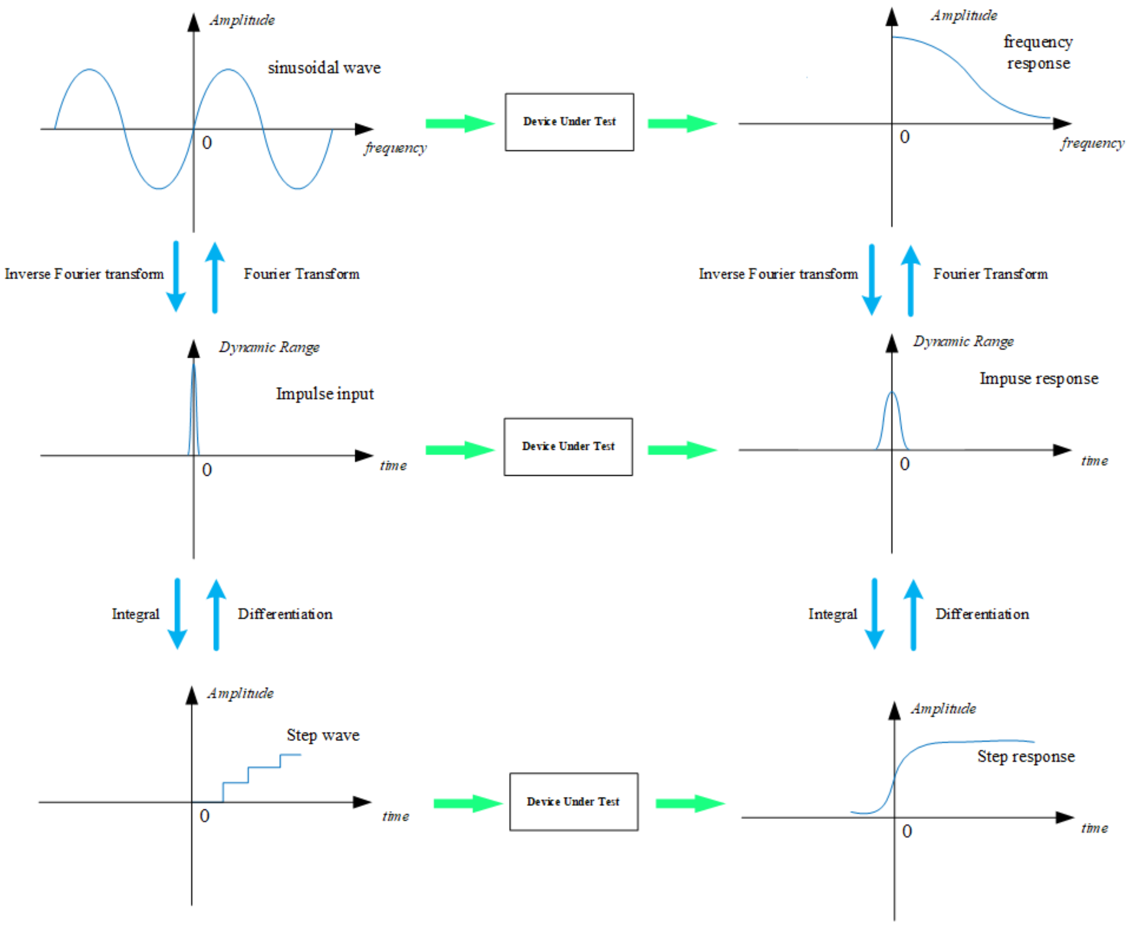

Figure 1. Relationship between frequency response, impulse response and step response [36,37].

2.2. Principle of Time-Frequency Conversion of Microwave Signal

Because the frequency domain data measured by the vector network analyzer are composed of discrete data, a linear frequency modulation Z transform (chirp-z transform) was adopted to obtain the corresponding time-domain response [38]. The chirp-z transform enables signal conversion to achieve uniform sampling on the helix of the Z plane which is suitable for channel prediction in the frequency domain. Because it can interpolate data points in the frequency domain, it can significantly improve the accuracy of the channel prediction [39]. In general, let the Z transformation of a finite length sequence be $x(n)$: this helix can start at any point in the Z plane and end at another arbitrary point, as shown in Equations (5)–(7).

$$X(zk) = \sum_{n=0}^{M-1} x(n) \times A^{-n} W^{nk}, k = 0, 1, \ldots, N-1, \tag{5}$$

where

$$A = A_0 exp(+jq_0), \tag{6}$$

$$W = W_0 exp(-jf0). \tag{7}$$

Equation (5) [40] defines the trend of the spiral line distributed on the Z plane as shown in Figure 2, where W_0 represents the extension rate of the helix, A_0 and θ_0 represents the starting sampling positions on the Z plane, and Φ_0 represents the bisection angle between the sampling points on the helix.

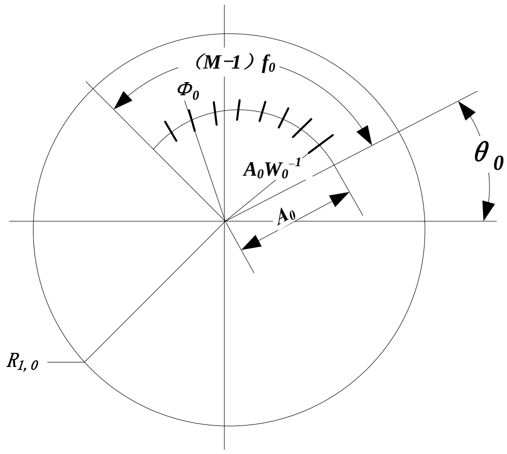

Figure 2. Schematic diagram of chirp-z transform sampling [41].

Substitute (6) and (7) into (5) to obtain Equation (8):

$$\begin{aligned} X(zk) = & \sum_{n=0}^{M-1} x(n)(A_0 exp(+j\theta_0))^{-n}(W_0 exp(+j\phi_0))^{nk} = \\ & \sum_{n=0}^{N-1} x(n) A_0^{-n} {W_0}^{nk} exp(-jn(\theta_0 + \phi_0)) \end{aligned} \tag{8}$$

The chirp-z transform is a common method for obtaining time-domain parameters from the measured S parameters. Kaiser–Bessel windowing was performed on the obtained S_{11} parameters [42]. Its window function is shown in Equation (9), where $W(n)$, represents the first kind of deformed zero-order Bessel function, and β represents a freely selectable parameter.

$$W(n) = \frac{I_0(\beta)\sqrt{1 - (1 - \frac{2n}{N-1})^2})}{I_0(\beta)} \tag{9}$$

The amplitude of the pulse waveform in the time domain response obtained by the chirp-z transformation was less than 1. Therefore, for the frequency domain response with non-zero edge data, the time domain result must be corrected using a scaling factor. The correct scaling factor of the corresponding time-domain transformation can be obtained by summing the window function as follows in Equation (10):

$$W_0 = \frac{\Delta\omega}{2\pi} \sum_{n=-N}^{N} W(n\Delta\omega), \tag{10}$$

where W is the Kaiser window function, $\Delta\omega$ represents the interval of frequency domain data dispersion, and W_0 represents the defined scaling factor. After normalization, the time-domain transformation becomes Equation (11):

$$f_{VNA}(t) = \frac{1}{W_0} \times \frac{\Delta\omega}{2\pi} \sum_{n=-N}^{N} F(n\Delta\omega) \times W(n\Delta\omega) \times e^{jn\Delta\omega t}, \tag{11}$$

where F (n Δ ω) is discrete frequency domain data.

Through the conversion and impedance changes of the time-domain and frequency-domain signals, the position of the impedance change signal in the frozen soil layer can be obtained to realize the accurate positioning of the frozen front in the actual measurement process.

2.3. Wave Crest Recognition Principle Based on Fourier Self-Deconvolution

To locate the frozen front clearly, it is necessary to quickly and accurately identify the peaks and valleys according to the map. In data processing of the chromatogram, spectrum, and electrochemical curve, the peak of the spectrum is easily affected by factors other than the object of study, resulting in peak stacking which makes it difficult to obtain more information from the spectrum curve [43]. Generally, there are 2 cases of wave peak overlap. The first type of spectral peak was close to complete overlap and the tip of each peak could not be identified. At this point, it was necessary to distinguish between each pea. The second type is affected by the number of sampling points and resolution of the atlas. The spectral peak is not easy to identify. At this point, the resolution of the atlas must be improved. Infrared absorption spectroscopy was used as an example. When the sample is irradiated by continuous wavelength infrared radiation, the molecule absorbs energy, transitions from the vibrational energy level ground state to the excited state, and generates a peak on the absorption curve, thus forming a complete infrared absorption spectrum. The collected curves are not infinitely fine because of the existence of molecular vibrations, which result in a low resolution of the spectrum and cannot be quickly identified. The Fourier self-deconvolution (FSD) method is widely used in analytical chemistry [44]. By further processing the infrared spectrum, the infrared spectrum peak can be divided into several peaks, effectively avoiding the interaction between peaks and increasing the accuracy and speed of wave peak recognition. In this study, the peak analysis function in Origin 2018 was used to identify wave peaks using the Fourier self-deconvolution method. The calculation principle is as follows.

The original spectrum was set as $A(\gamma)$, the resolution after the sub-package treatment is $B(\gamma)$, and the resolution spectrum can be determined by the linear function $G(\gamma)$ which is the same as the original spectrum $A(\gamma)$ There is a mathematical deconvolution system between them, namely Equation (12):

$$A(\gamma) = G(\gamma) \cdot B(\gamma) = \int_{-\infty}^{+\infty} G(\gamma)B(\gamma - x)dx. \tag{12}$$

The required resolution spectrum B can be using the inverse Fourier transform of Equation (12), $B(\gamma)$, from $F^{-1}\{B(\gamma)\} = F^{-1}\{G(\gamma)\} \cdot F^{-1}\{B(\gamma)\}$ existence relation: $F^{-1}\{B(\gamma)\} = \frac{F^{-1}\{A(\gamma)\}}{F^{-1}\{G(\gamma)\}}$, then $B(\gamma)$ can be rewritten as Equation (13):

$$B(\gamma) = F\{\frac{F^{-1}\{A(\gamma)\}}{F^{-1}\{G(\gamma)\}}\}, \tag{13}$$

where $G(\gamma)$ is generally the Lorentz function, namely Equation (14):

$$G(\gamma) = \frac{\delta}{\pi(\gamma^2 - \delta^2)}, F^{-1}\{G(\gamma)\} = G(\gamma) \cdot e^{-2\pi\delta|x|}, \tag{14}$$

where δ is the half-peak width of the Lorentz function. Take 1 in this manuscript.

3. Test Plan for Frozen Soil Frontal Detection Based on TDR

The traditional TDR method measures the relevant characteristics of a medium by measuring the propagation characteristics of the electromagnetic waves in the medium. When electromagnetic waves propagate in a medium, they are influenced by factors such as the moisture content and dielectric constant, thereby changing the propagation speed and reflection intensity of electromagnetic waves. The TDR instrument calculated the water content and movement status of the soil by sending electromagnetic waves and measuring the time and intensity of the reflected signal. During the freezing process, as the soil temperature decreases, water will gradually freeze to form an ice phase, which changes the dielectric constant of the soil, thereby changing the propagation speed and reflection intensity of electromagnetic waves. This study first sets a soil sample with an initial moisture content of 30%, pre-freezes a portion of the sample length, and tightly fits it with the unfrozen soil sample. The experiment was conducted using a TDR100 time-domain reflectometer and a self-made PCB probe at different freezing depths, the physical image of which is shown in Figure 3, and the experimental phenomena were observed and analyzed. In this study, the soil types in four regions of China are selected, according to the "Standard for Geotechnical Testing Method (GB/T 50123-2019)" [45]. The soil sand silt clay content is determined by laser particle size analyzer, the soil classification is carried out according to the triangular coordinate map of soil texture made in the United States, and the soil filling density is determined by the vibrating hammering method in order to configure different gradient volume moisture content. The physical properties of the black soil used in the experiment are listed in Table 1.

Figure 3. Physical image of the probe.

Table 1. Physical properties of black soil.

Soil	Cosmid (%) (<0.002 mm)	Powder (%) (0.002–0.02 mm)	Sand Grain (%) (0.02–2 mm)	Bulk Density (g/cm^3)
Black soil	19.44	22.32	58.24	1.31

The equipment used in the experiment is shown in Table 2.

Table 2. TDR Frozen Frontal Experimental Monitoring System.

Experimental Equipment	Model
Time Domain Reflectometer	Campbell scientific TDR100, Logan, UT, USA
DC power supply	TECPEL UTP-3305, Taipei, China
Homemade PCB probe	—
Adapter cable	ADL BNC-SMACable, Shenzhen, China

TECPEL UTP-3305 DC power supply was inserted into a 220 V power outlet, the power output line was connected to the power interface of the Campbell TDR100, and the power voltage and current were set to 12 V and 0.6 A, respectively to ensure the normal operation of the TDR100. The TDR interface was connected to a self-made PCB probe using an ADL BNC-SMA cable. TDR100 was started and PC-TDR software was used to monitor the frozen front. When performing measurement using software, it is necessary to set appropriate monitoring parameters for the measurement window. In this study, the communication baud rate was set to 57,600, the window length was 2 m, the probe length was 0.2 m, the number of sampling points was 1024, and the specified unit detection constant was set to 1. The monitoring program was started, and the monitoring results were awaited. The monitoring results were viewed using software and the data were exported to a computer for further processing and analysis.

The experimental results obtained by setting different freezing depths on black soil and conducting TDR measurements are shown in Figure 4.

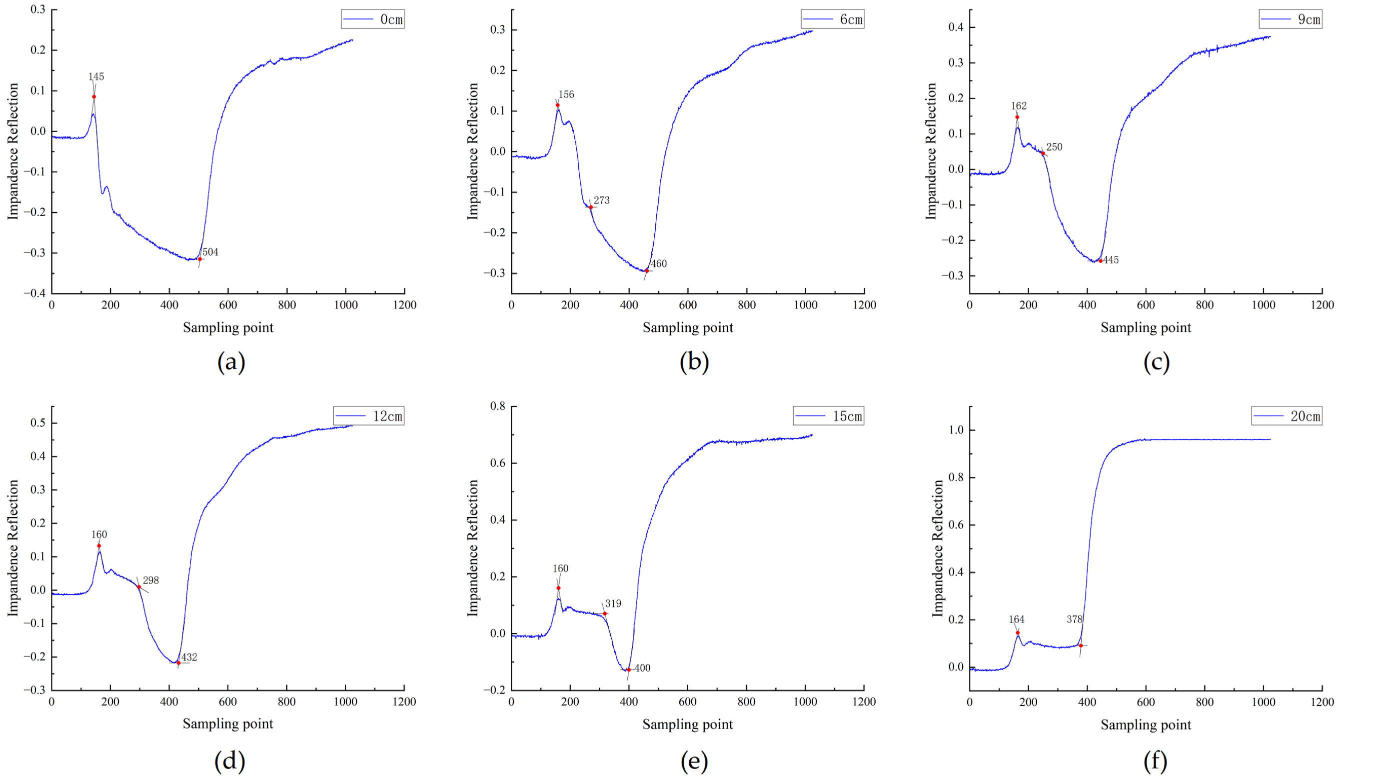

Figure 4. TDR100 Frozen Front Experimental Results. (**a**) 0 cm; (**b**) 6 cm; (**c**) 9 cm; (**d**) 12 cm; (**e**) 15 cm; (**f**) 20 cm.

As shown in Figure 4, as the thickness of the frozen soil layer increased, the reflection point at the end of the TDR probe signal shifted forward. This is because the transmission speed of the signal in the probe is related to the environment of the medium. As the thickness of the frozen soil increases, the water content in the soil sample decreases, leading to an increase in the propagation speed of the signal wave in the soil and causing the reflection point at the end to move forward. At the same time, it is also noted that the position of the intermediate signal reflection point increases with the depth of the frozen front. This is consistent with the change in the position of the frozen front, but the rising edge of the reflection point is large, and the position of the reflection point needs to be manually determined using the tangent method. This process is cumbersome, complex, and is greatly influenced by subjective factors. Therefore, this study conducted freezing front experiments on four soils using I-TDR technology.

4. Test Plan for Frozen Soil Frontal Detection Based on I-TDR

To explore the adaptability of I-TDR technology in measuring the freezing front of different soil types, four soil samples with different textures (sand, loess, black soil, and red soil) were selected for the test. The sand was taken from the vicinity of the Weihe Wetland Park, Yangling District, Xianyang City, Shaanxi Province (108°09′ N, 34°24′ E). The soil was loose and has good water permeability but has poor water and fertilizer retention capacity, and the soil depth was 30–40 cm; Loess was taken from the vicinity of Xiaojiahe Village, Yujiawan Town, Zichang County, Yan'an City, Shaanxi Province (109°67′ E, 37°13′ N, 1324 m above sea level). The content of sand particles in the soil accounted for 1/3, the soil viscosity was moderate, and the soil depth was 30–40 cm; Black soil was taken from Tieling City, Liaoning Province (124°02′ E, 43°16′ N) in a hilly area with soil granular structure, loose soil, many plant roots, high soil fertility, and a soil depth of 20–30 cm; Red soil was collected in Qujing City, northeastern Yunnan Province (103°85′ E, 25°46′ N, altitude 2052 m). The soil was small, granular, easily absorbed water, and had a depth of 30–40 cm. The physical properties of the other samples except for black soil are shown in Table 3.

Table 3. Physical properties of four different texture soils.

Soil	Cosmid (%) (<0.002 mm)	Powder (%) (0.002–0.02 mm)	Sand Grain (%) (0.02–2 mm)	Bulk Density (g/cm^3)
Sand	8.08	20.36	71.56	1.54
Loess	12.46	50.32	37.22	1.70
Red soil	28.53	42.56	28.91	1.46

After natural air drying, grinding, and impurity removal, the four types of soil were screened with an 18-mesh sieve (aperture 1 mm), dried in an oven at 105 °C for 24 h, and stored on standby. After winter irrigation, farmland soil often exhibits high moisture content, and considering the influence of phase change latent heat on permafrost, high moisture content soil was selected as the research object in this study. According to the filling density of each soil sample, deionized water was used to prepare soil samples with an initial moisture content of 30%. To reduce the impact of the ambient temperature on the test piece, the test piece preparation process was performed at a room temperature of 24 ± 2 °C. The configured soil samples were left standing for 8 h and then filled with PVC tubes (4.65 cm in diameter and 21 cm in height) after the moisture distribution was uniform. Considering that it is not convenient to insert probes after the soil is frozen, the probe was inserted into the frozen soil layer before freezing, and the PVC tubes were wrapped with a thermal insulation foam layer using the one-way freezing method and then frozen in a −30 °C incubator for 12 h. The probe was removed and tightly fitted with an unfrozen test piece, as shown in Figure 5a.

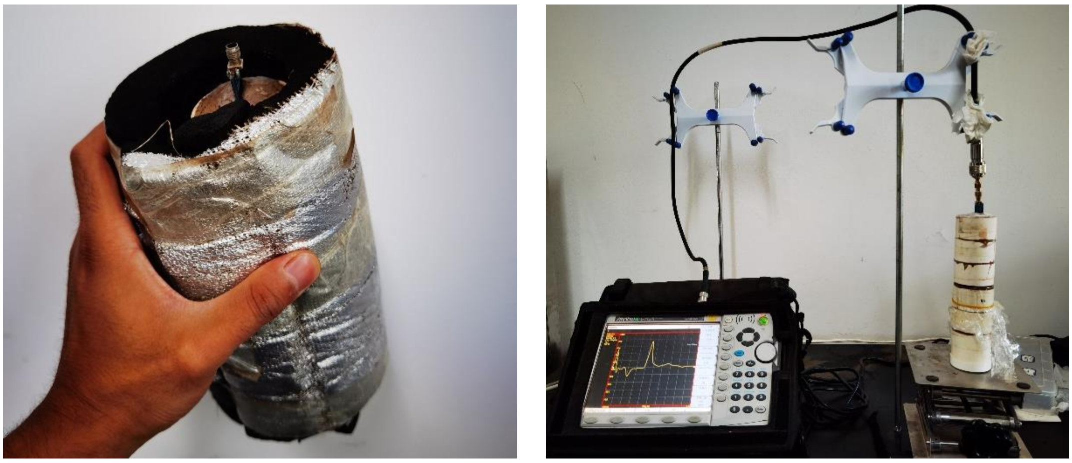

(**a**) (**b**)

Figure 5. Picture of sample and experimental system. (**a**) Sample preparation (**b**) Physical drawing of the measuring system.

The filling heights of the upper frozen soil (30% moisture content) in the two layers of the soil column were 0, 6, 9, 12, 15, and 20 cm. The upper frozen soil layer and lower wet soil layer were separated using fresh film, as shown in Figure 5b. A schematic diagram of the soil samples at different freezing depths is shown in Figure 6.

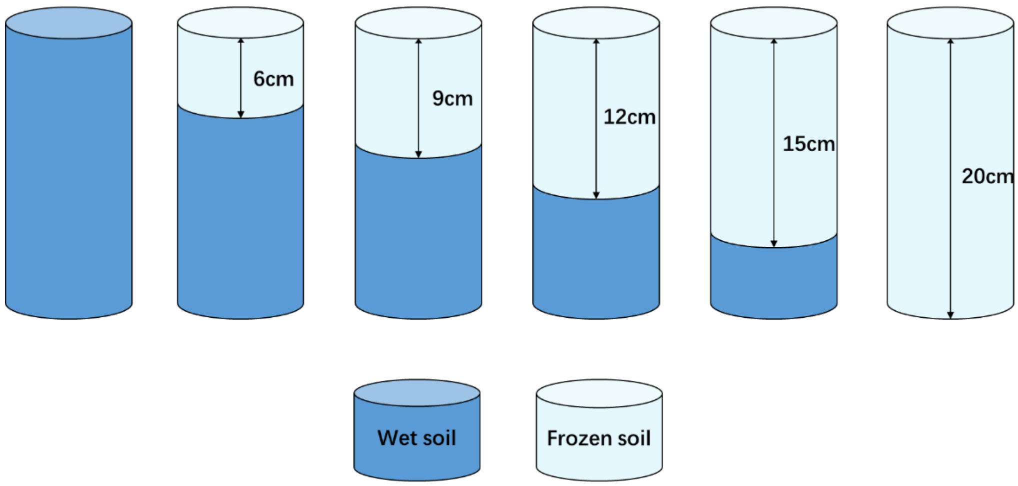

Figure 6. Schematic diagram of the sample preparation.

The model of the vector network analyzer used in the test was Anritsu-MS2028B, the probe was a 20 cm self-made probe. The number of sampling points was 1024, and the measurement frequency range was set to 1 MHz~6 GHz. Before the test, the vector network analyzer was calibrated using the SOLT calibration method [46], and the average value was obtained for three measurements of each soil sample. Three portions of soil with different water content were dried, and the actual water content of the prepared soil sample was calculated.

The probe used in this study was a three-pin PCB probe with a length of 200 mm and a width of 20 mm. Three copper foil strips, each 200 mm long, 4 mm wide, and 4 mm apart, were placed on the PCB. The DUT is to be measured through a 50 Ω coaxial cable, and the equipment outputs a frequency sweep signal of 1 MHz~6 GHz to the probe. If the environmental impedance of the sensor to be measured is discontinuous, reflection occurs and the reflected signal is sampled. The equipment measured the reflected signal of the frozen peak surface to obtain the impedance reflection coefficient, and the impedance measurement was realized. After time domain conversion, the discontinuous points of the soil impedance can be accurately located, and the depth of the frozen soil layer can be measured. Figure 7 shows the design and signal measurement principles.

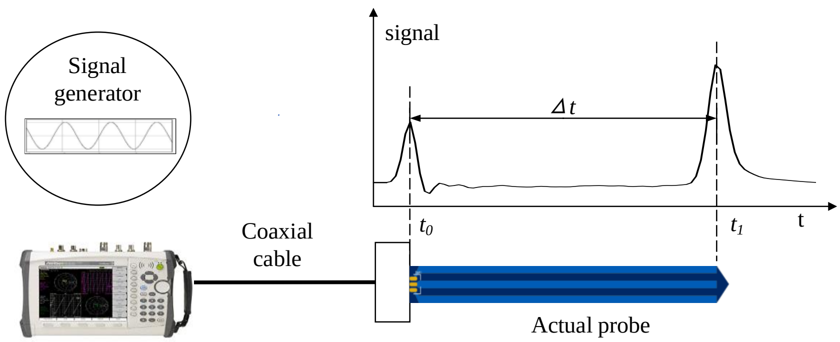

Figure 7. Schematic diagram of the probe measurement signal.

5. Result and Discussion

Data processing and mapping were performed using Origin 2018 and MATLAB 2019b. The determination coefficient (R^2) and root mean square error (RMSE) were used to analyze the linear correlation between the preset depth of the soil freezing front and the measured value of the soil freezing depth obtained using the Anritsu-MS2028B vector network analyzer. The closer R^2 is to one, the smaller the RMSE and the more accurate the measurement model is.

The Anritsu-MS2028B vector network analyzer and self-made probe were used to measure sand, loess, black soil, and red soil with four different textures at freezing depths of 0, 6, 9, 12, 15, and 20 cm, respectively. The waveforms of the first 800 sampling points of each frozen front depth were drawn as shown in Figure 8.

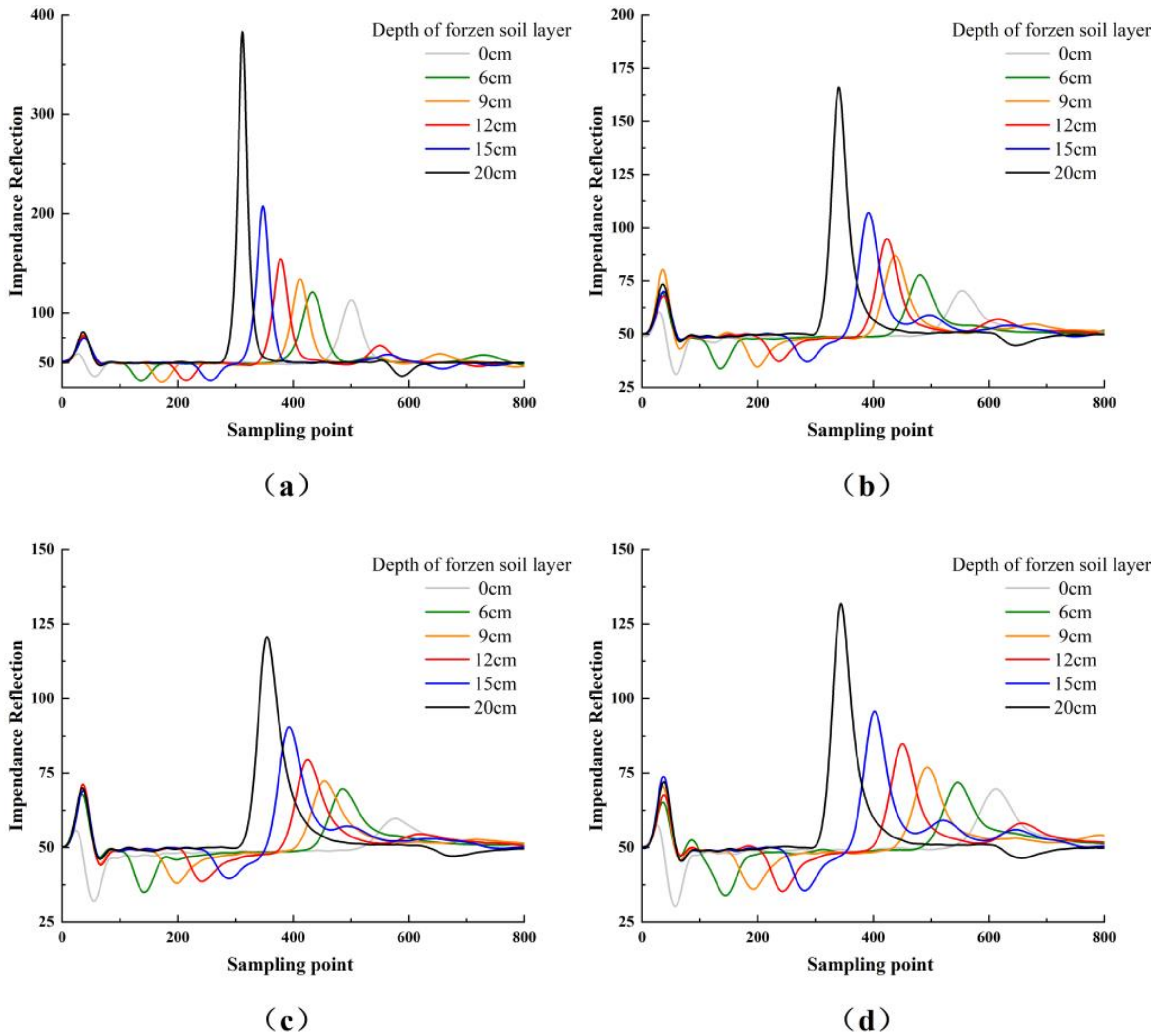

Figure 8. Combined measurement of frozen front in different depths of 4 soils. (**a**) Sand; (**b**) Loess; (**c**) Black soil; (**d**) Red soil.

It can be observed from Figure 8 that the four types of soils are generally consistent in the measurement process of the freezing front at different depths. The electromagnetic wave is reflected for the first time at the interface of air and soil through the coaxial line, and this reflection is shown as the initial wave peak of the TDR in the impedance diagram. When an electromagnetic wave propagates to the interface between frozen soil and unfrozen soil, owing to the change in medium impedance, the electromagnetic wave is reflected in the transmission process, forming a reflected wave valley whose reflection point is the location of the frozen front of the soil. Because soil samples with different volumes of water content have different dielectric constants [47], in the same soil, with the deepening of the frozen front, the overall volume of water content decreases, the propagation speed of electromagnetic waves increases, and the reflection point at the end of the probe moves forward. To express the valley value movement soil impedance with the change in soil freezing depth more clearly, the measurement waveforms of different freezing depths of each soil were drawn, as shown in Figure 9.

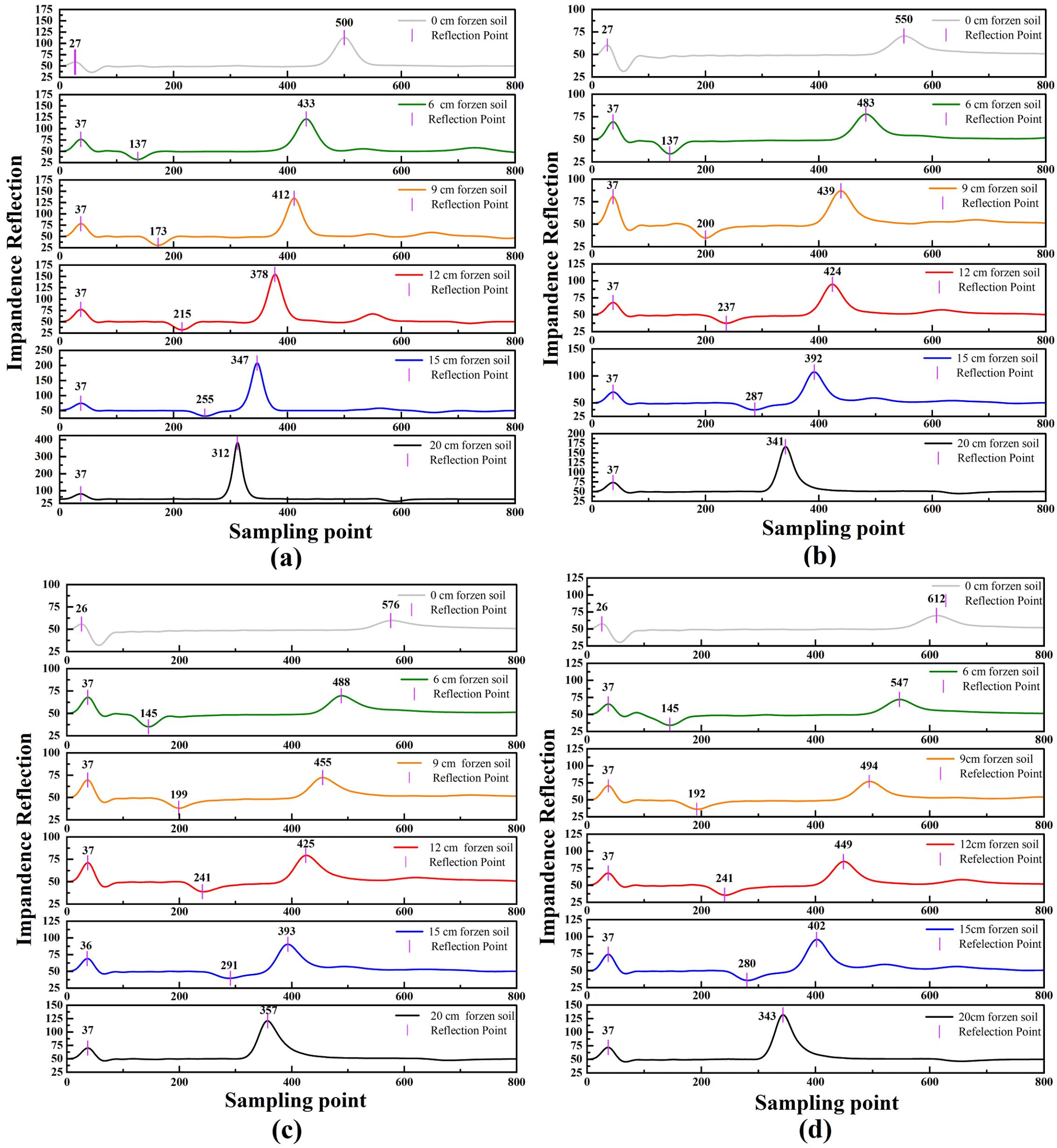

Figure 9. Single wave measurements of different frozen front depths of the 4 soils. (**a**) Sand; (**b**) Loess; (**c**) Black soil; (**d**) Red soil.

Combining Figures 3 and 9c, it can be clearly observed that the I-TDR method can more intuitively reflect the soil freezing front. As shown in Figure 9, the initial reflection points of sand, loess, black soil, and red soil with four different textures are 27, 27, 26, and 26, respectively, when the frozen soil depth is 0. At this time, the accidental error caused by improper control of the probe insertion depth during the preparation of this part of the test piece was considered. Most of the initial reflection points of the frozen upper soil were located at the 37th sampling point. It is mainly considered that when preparing the frozen soil sample, the probe has been pre-inserted into the sample, and the upper part of the probe is still exposed to the air. During the freezing process, the water vapor in the air condenses on the surface of the upper probe, causing the propagation rate of the electromagnetic wave to decrease, thus causing the initial reflection point to move backward. This phenomenon is consistent with the experimental phenomenon of verifying the Lewis number [48], which further explains that the temperature of the plate decreases, and the moisture in the air condenses on the surface of the plate. When the frozen depth of the black soil reached 15 cm, the initial reflection point was the 36th reflection point, which was also considered an accidental error in the preparation of the test piece. When there was no frozen front in the four types of soil, the environment of the probe was a uniform medium, the impedance did not change, and the obtained waveform included only the wave peaks of the two reflection points at the beginning and end of the probe. When the permafrost layer was 6, 9, 12, and 15 cm, the physical state of the soil moisture in the layer of the probe was different, resulting in a change in the transmission medium, the discontinuous change in impedance, and the reflection of the primary electromagnetic wave. Because the impedance of the upper permafrost layer is large, and the impedance of the lower wet soil layer is small, according to the calculation formula of the impedance reflection coefficient, a reflection wave trough of the frozen front is formed between the initial wave peak and the end reflection point, the location of each sampling point is shown in Table 4.

Table 4. The position of the starting reflection point, middle reflection point, and end reflection point of the 4 soils with different depths of frozen soil.

Soil Type / Depth	Reflection Point Type	0 cm	6 cm	9 cm	12 cm	15 cm	20 cm
Sand	Starting point of reflection	27	37	37	37	37	37
	Intermediate reflection point		137	173	215	255	
	End reflection point	500	433	412	378	347	312
Loess	Starting point of reflection	27	37	37	37	37	37
	Intermediate reflection point		137	200	237	287	
	End reflection point	550	483	439	424	392	341
Black earth	Starting point of reflection	26	37	37	37	36	37
	Intermediate reflection point		145	199	241	291	
	End reflection point	576	488	455	425	393	357
Red soil	Starting point of reflection	26	37	37	37	37	37
	Intermediate reflection point		145	192	241	280	
	End reflection point	612	547	494	449	402	343

It can be observed from Table 4 that for soil samples with a freezing depth of 0 cm, the initial reflection point is slightly different. This is because, as mentioned above, the end reflection point gradually increases with the soil sample number, owing to the increase in clay content and the increase in soil particle adsorption to water, resulting in a decrease in the electromagnetic wave speed during the transmission process. Thus, the end reflection point moves backward.

The distance between the initial reflection point and the reflection point at the end of the probe was used as the probe length to normalize the obtained soil waveform sampling points using Equation (15), and the measured value d at different freezing depths was obtained Equation (15):

$$d = \left(\frac{X_i - X_a}{X_b - X_a}\right) \cdot L \cdot 100\% \tag{15}$$

where L—probe length

X_a—starting reflection point position

X_b—position of the end reflection point

X_i—frozen front reflection point position

The measurement results of black soil TDR and I-TDR using (16) to obtain the frozen soil depth measurement value, and the error with the true value. RMSE is selected as the evaluation standard, and the results are shown in Figure 10.

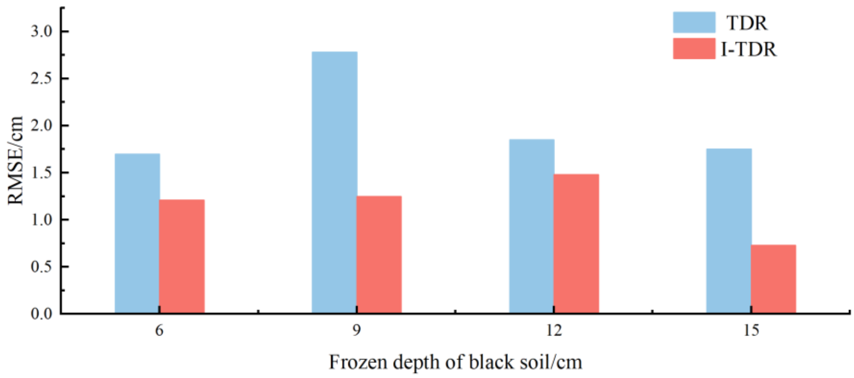

Figure 10. Comparison of measurement errors between I-TDR and TDR.

From Figure 10, it can be observed that compared to the TDR method for measuring soil freezing depth, the measurement error based on the I-TDR method is significantly reduced at all measurement positions, with the RMSE difference reaching 1.23 cm at the 9 cm measurement point. This indicates that the method based on I-TDR is more effective than the traditional TDR method in measuring soil freezing depth.

To analyze the adaptability of I-TDR method to different soil samples, the actual set soil freezing depth was taken as the ordinate and the measured value of the soil freezing front obtained by the normalization method was used as the ordinate to fit the positions of the four different texture soil freezing fronts, as shown in Figure 11.

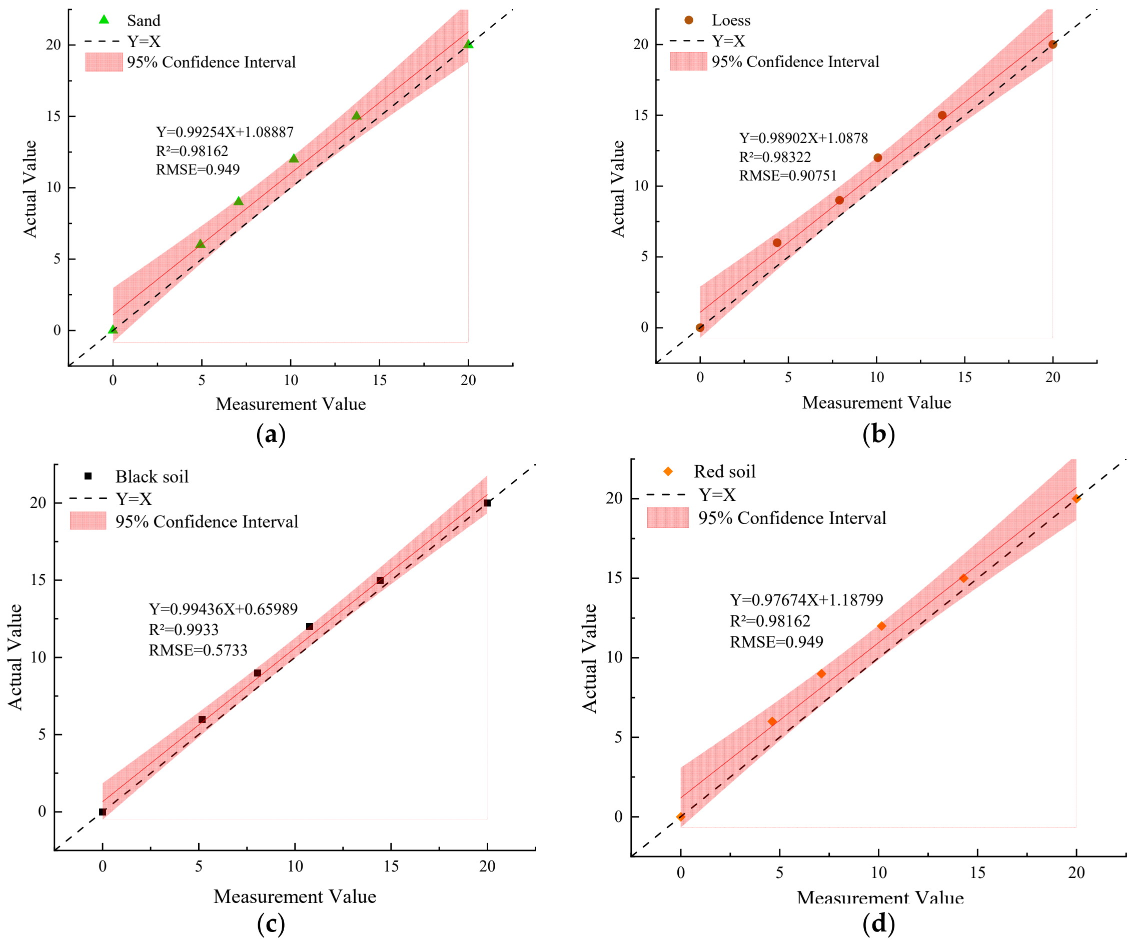

Figure 11. Correlation check of freezing depth. (**a**) Sand; (**b**) Loess; (**c**) Black soil; (**d**) Red soil.

As shown in Figure 11, the data points were located above the Y = X calibration line, indicating that the measured value of the frozen front was generally less than the true value. However, through the linear fitting of the measured value and setting the 95% confidence interval, it can be seen that the measured data points and the Y = X calibration line is within the 95% confidence interval of the measurement model, which indicates that the model has a high degree of fit and meets the experimental requirements. Furthermore, from Figure 11, it can be concluded that the determination coefficients of the actual and measured values of the fitting results of the four different texture soils reached more than 0.98, with excellent correlation, and the root mean square error was less than 1 cm, in which the RMSE of the black soil was 0.573, and the error values of the four soil sample measurement were less than 5%, indicating that the fitting results and the actual results had a high correlation, the measurement method was effective, and could be used to accurately locate the location of the soil freezing front. Therefore, the position of the freezing front of different types of soils can be accurately measured using I-TDR technology.

There are still several points to note when using the I-TDR method mentioned in the text to monitor the depth of permafrost layers. During the experiment, it was found that the initial reflection points of the entire unfrozen soil moved forward compared with that of the upper frozen soil and lower unfrozen soil, mainly considering the influence of water vapor in the air on the measurement of the upper part of the probe after freezing, which should be considered in practical applications. In this study, the measured value of soil freezing depth based on I-TDR technology was generally less than the actual value, and the measuring point error was within 5%. In the future, further research on probe structure and measurement methods to further improve measurement accuracy. To explore the feasibility of applying the I-TDR method to monitoring the depth of frozen soil, this study was only conducted under laboratory conditions. In the future, other methods will be considered to conduct in situ experiments on the depth of frozen soil.

6. Conclusions

Based on the principle of impedance reflection and time-frequency conversion, this study proposes a method to accurately measure the frozen front of soil using I-TDR technology. A vector network analyzer was used to transmit sine excitation signals with constant amplitude, wide measurement frequency band, high resolution, and minimal influence from external factors. The single wave analysis of the soil impedance waveform was performed using the method of frequency domain to the time-domain. Through the test setup and comparison, the results showed that the change in the soil freezing front depth based on the I-TDR technology was sensitive and reliable. The measurement correlation coefficient of the four types of soil freezing depths exceeded 0.98, and the measurement error was within 5%. This provides a method for automatic and intelligent monitoring of frozen soil depth, changes the disadvantages of traditional frozen soil depth monitoring, which is time-consuming, laborious, and inaccurate, and is of great significance for reflecting regional climate change through frozen soil depth, engineering surveys in cold regions, and guiding agricultural irrigation in winter.

Author Contributions: Research conceptualization, H.Q. and J.X.; data curation, H.Q. and Z.M.; methodology, H.Q. and J.X.; writing—original draft, H.Q.; writing—review and editing, J.X., X.J., X.L. and Q.K. All authors have read and agreed to the published version of the manuscript.

Funding: This research was funded by the National Natural Science Foundation of China (Grant No. 52279046).

Data Availability Statement: Not applicable.

Conflicts of Interest: The authors declare no conflict of interest.

References

1. Zhang, Z.; Ma, W.; Zhang, Z. Scientific Concept and Application of Frozen Soil Engineering System. *Cold Reg. Sci. Technol.* **2018**, *146*, 127–132. [CrossRef]
2. Henry, H.A.L. Climate Change and Soil Freezing Dynamics: Historical Trends and Projected Changes. *Clim. Chang.* **2008**, *87*, 421–434. [CrossRef]
3. Zheng, X.Q.; Van Liew, M.W.; Flerchinger, G.N. Experimental Study of Infiltration into a Bean Stubble Field during Seasonal Freeze-Thaw Period. *Soil Sci.* **2001**, *166*, 3–10.
4. Chen, J.; Xie, X.; Zheng, X.; Xue, J.; Miao, C.; Du, Q.; Xu, Y. Effect of Straw Mulch on Soil Evaporation during Freeze-Thaw Periods. *Water* **2019**, *11*, 1689. [CrossRef]
5. Orakoglu, M.E.; Liu, J.; Tutumluer, E. Frost Depth Prediction for Seasonal Freezing Area in Eastern Turkey. *Cold Reg. Sci. Technol.* **2016**, *124*, 118–126. [CrossRef]
6. Gao, J.; Xie, Z.; Wang, A.; Liu, S.; Zeng, Y.; Liu, B.; Li, R.; Jia, B.; Qin, P.; Xie, J. A New Frozen Soil Parameterization Including Frost and Thaw Fronts in the Community Land Model. *J. Adv. Model. Earth Syst.* **2019**, *11*, 659–679. [CrossRef]
7. Ming, F.; Li, D. A Model of Migration Potential for Moisture Migration during Soil Freezing. *Cold Reg. Sci. Technol.* **2016**, *124*, 87–94. [CrossRef]
8. Zhang, Y.; Horton, R.; White, D.J.; Vennapusa, P.K.R. Seasonal Frost Penetration in Pavements with Multiple Layers. *J. Cold Reg. Eng.* **2018**, *32*, 05018002. [CrossRef]
9. Sharratt, B.S. Freeze-Thaw and Winter Temperature of Agricultural Soils in Interior Alaska. *Cold Reg. Sci. Technol.* **1993**, *22*, 105–111. [CrossRef]
10. Peng, X.; Frauenfeld, O.W.; Cao, B.; Wang, K.; Wang, H.; Su, H.; Huang, Z.; Yue, D.; Zhang, T. Response of Changes in Seasonal Soil Freeze/Thaw State to Climate Change from 1950 to 2010 across China: Soil Seasonal Freeze/Thaw State Changes. *J. Geophys. Res. Earth Surf.* **2016**, *121*, 1984–2000. [CrossRef]
11. Musa, A.; Ya, L.; Anzhi, W.; Cunyang, N. Characteristics of Soil Freeze–Thaw Cycles and Their Effects on Water Enrichment in the Rhizosphere. *Geoderma* **2016**, *264*, 132–139. [CrossRef]
12. Xiao, Z.; Lai, Y.; Zhang, M. Study on the Freezing Temperature of Saline Soil. *Acta Geotech.* **2018**, *13*, 195–205. [CrossRef]
13. Wang, D.; Wang, Y.; Ma, W.; Lei, L.; Wen, Z. Study on the Freezing-Induced Soil Moisture Redistribution under the Applied High Pressure. *Cold Reg. Sci. Technol.* **2018**, *145*, 135–141. [CrossRef]
14. Wang, C.; Lai, Y.; Zhang, M. Estimating Soil Freezing Characteristic Curve Based on Pore-Size Distribution. *Appl. Therm. Eng.* **2017**, *124*, 1049–1060. [CrossRef]
15. Flerchinger, G.N.; Saxton, K.E. Simultaneous Heat and Water Model of a Freezing Snow-Residue-Soil System II. Field Verification. *Trans. ASAE* **1989**, *32*, 573–576. [CrossRef]
16. Flerchinger, G.N.; Saxton, K.E. Simultaneous Heat and Water Model of a Freezing Snow-Residue-Soil System I. Theory and Development. *Trans. ASAE* **1989**, *32*, 565–571. [CrossRef]
17. Bao, H.; Koike, T.; Yang, K.; Wang, L.; Shrestha, M.; Lawford, P. Development of an Enthalpy-Based Frozen Soil Model and Its Validation in a Cold Region in China: An Enthalpy-Based Frozen Soil Model. *J. Geophys. Res. Atmos.* **2016**, *121*, 5259–5280. [CrossRef]
18. Iwata, Y.; Hirota, T.; Suzuki, T.; Kuwao, K. Comparison of Soil Frost and Thaw Depths Measured Using Frost Tubes and Other Methods. *Cold Reg. Sci. Technol.* **2012**, *71*, 111–117. [CrossRef]
19. Aleksic, S.O.; Mitrovic, N.S.; Lukovic, M.D.; Veljovic-Jovanovic, S.D.; Lukovic, S.G.; Nikolic, M.V.; Aleksic, O.S. A Ground Temperature Profile Sensor Based on NTC Thick Film Segmented Thermistors: Main Properties and Applications. *IEEE Sens. J.* **2018**, *18*, 4414–4421. [CrossRef]
20. Wu, B.; Zhu, H.-H.; Cao, D.; Xu, L.; Shi, B. Feasibility Study on Ice Content Measurement of Frozen Soil Using Actively Heated FBG Sensors. *Cold Reg. Sci. Technol.* **2021**, *189*, 103332. [CrossRef]
21. Zhan, W.; Zhou, J.; Ju, W.; Li, M.; Sandholt, I.; Voogt, J.; Yu, C. Remotely Sensed Soil Temperatures beneath Snow-Free Skin-Surface Using Thermal Observations from Tandem Polar-Orbiting Satellites: An Analytical Three-Time-Scale Model. *Remote Sens. Environ.* **2014**, *143*, 1–14. [CrossRef]
22. Leger, E.; Dafflon, B.; Soom, F.; Peterson, J.; Ulrich, C.; Hubbard, S. Quantification of Arctic Soil and Permafrost Properties Using Ground-Penetrating Radar and Electrical Resistivity Tomography Datasets. *IEEE J. Sel. Top. Appl. Earth Obs. Remote Sens.* **2017**, *10*, 4348–4359. [CrossRef]
23. Sudisman, R.A.; Osada, M.; Yamabe, T. Heat Transfer Visualization of the Application of a Cooling Pipe in Sand with Flowing Pore Water. *J. Cold Reg. Eng.* **2017**, *31*, 04016007. [CrossRef]
24. Sveen, S.-E.; Nguyen, H.T.; Sørensen, B.R. Soil Moisture Variations in Frozen Ground Subjected to Hydronic Heating. *J. Cold Reg. Eng.* **2020**, *34*, 04020025. [CrossRef]
25. Qin, Y.; Wang, Q.; Xu, D.; Yan, J.; Zhang, S. A Fiber Bragg Grating Based Earth and Water Pressures Transducer with Three-Dimensional Fused Deposition Modeling for Soil Mass. *J. Rock Mech. Geotech. Eng.* **2022**, *14*, 663–669. [CrossRef]
26. Liu, Z.; Gu, X.; Wu, C.; Ren, H.; Zhou, Z.; Tang, S. Studies on the Validity of Strain Sensors for Pavement Monitoring: A Case Study for a Fiber Bragg Grating Sensor and Resistive Sensor. *Constr. Build. Mater.* **2022**, *321*, 126085. [CrossRef]
27. Cao, D.; Zhu, H.; Wu, B.; Wang, J.; Shukla, S. Investigating Temperature and Moisture Profiles of Seasonally Frozen Soil under Different Land Covers Using Actively Heated Fiber Bragg Grating Sensors. *Eng. Geol.* **2021**, *290*, 106197. [CrossRef]

28. Colliander, A.; Reichle, R.; Crow, W.; Cosh, M.; Chen, F.; Chan, S.; Das, N.N.; Bindlish, R.; Chaubell, J.; Kim, S.; et al. Validation of Soil Moisture Data Products From the NASA SMAP Mission. *IEEE J. Sel. Top. Appl. Earth Obs. Remote Sens.* **2022**, *15*, 364–392. [CrossRef]
29. Wu, S.; Zhao, T.; Pan, J.; Xue, H.; Zhao, L.; Shi, J. Improvement in Modeling Soil Dielectric Properties during Freeze-Thaw Transitions. *IEEE Geosci. Remote Sens. Lett.* **2022**, *19*, 2001005. [CrossRef]
30. Zhang, T.; Jiang, L.; Zhao, S.; Chai, L.; Li, Y.; Pan, Y. Development of a Parameterized Model to Estimate Microwave Radiation Response Depth of Frozen Soil. *Remote Sens.* **2019**, *11*, 2028. [CrossRef]
31. Liu, Z.; Gu, X.; Wu, W.; Zou, X.; Dong, Q.; Wang, L. GPR-Based Detection of Internal Cracks in Asphalt Pavement: A Combination Method of DeepAugment Data and Object Detection. *Measurement* **2022**, *197*, 111281. [CrossRef]
32. Zhang, L.; Zhao, T.; Jiang, L.; Zhao, S. Estimate of Phase Transition Water Content in Freeze-Thaw Process Using Microwave Radiometer. *IEEE Trans. Geosci. Remote Sens.* **2010**, *48*, 4248–4255. [CrossRef]
33. Jadoon, K.; Weihermüller, L.; McCabe, M.; Moghadas, D.; Vereecken, H.; Lambot, S. Temporal Monitoring of the Soil Freeze-Thaw Cycles over a Snow-Covered Surface by Using Air-Launched Ground-Penetrating Radar. *Remote Sens.* **2015**, *7*, 12041–12056. [CrossRef]
34. Vetterli, M.; Kovačević, J.; Goyal, V.K. *Foundations of Signal Processing*; Cambridge University Press: Cambridge, UK, 2014; ISBN 978-1-107-03860-8.
35. Lin, C.P. Analysis of Nonuniform and Dispersive Time Domain Reflectometry Measurement Systems with Application to the Dielectric Spectroscopy of Soils: Analysis of TDR Measurements. *Water Resour. Res.* **2003**, *39*, 1–11. [CrossRef]
36. Zhu, Y.; Gao, T.; Fan, X.; Han, F.; Wang, C. Electrochemical Techniques for Intercalation Electrode Materials in Rechargeable Batteries. *Acc. Chem. Res.* **2017**, *50*, 1022–1031. [CrossRef]
37. Voyagaki, E.; Mylonakis, G.; Psycharis, I.N. Sliding Blocks under Near-Fault Pulses: Closed-Form Solutions. In *Geotechnical Earthquake Engineering and Soil Dynamics IV*; American Society of Civil Engineers: Sacramento, CA, USA, 2008; pp. 1–10.
38. Heim Weber, G.; de Moura, H.L.; Pipa, D.R.; Martelli, C.; da Silva, J.C.C.; da Silva, M.J. Cable Fault Characterization by Time-Domain Analysis From S-Parameter Measurement and Sparse Inverse Chirp-Z Transform. *IEEE Sens. J.* **2021**, *21*, 1009–1016. [CrossRef]
39. Tan, S.; Hirose, A. Low-Calculation-Cost Fading Channel Prediction Using Chirp Z-Transform. *Electron. Lett.* **2009**, *45*, 418. [CrossRef]
40. Bellanger, M. Digital processing of signals: Theory and practice. In *Digital Processing of Signals: Theory and Practice*; John Wiley & Sons: New York, NY, USA, 2000; ISBN 978-0-471-97673-8.
41. Chang, L.; Cui, G. Moiré Fringe Phase Difference Measurement Based on Spectrum Zoom Technology. *Telkomnika Indones. J. Electr. Eng.* **2013**, *11*, 6025–6033. [CrossRef]
42. Lewitt, R.M. Multidimensional Digital Image Representations Using Generalized Kaiser–Bessel Window Functions. *J. Opt. Soc. Am. A* **1990**, *7*, 1834. [CrossRef]
43. Qian, F.; Wu, Y.; Hao, P. An Automated Algorithm of Peak Recognition Based on Continuous Wavelet Transformation and Local Signal-to-Noise Ratio. *Appl. Spectrosc.* **2017**, *71*, 1947–1953. [CrossRef]
44. Lorenz-Fonfria, V.A.; Padros, E. The Role and Selection of the Filter Function in Fourier Self-Deconvolution Revisited. *Appl. Spectrosc.* **2009**, *63*, 791–799. [CrossRef] [PubMed]
45. *GB/T 50123–2019*; Standard for Geotechnical Testing Method. National Standards of P.R.C.: Beijing, China, 2019.
46. Zhao, W.; Qin, H.-B.; Qiang, L. A Calibration Procedure for Two-Port VNA with Three Measurement Channels Based on t-Matrix. *Prog. Electromagn. Res. Lett.* **2012**, *29*, 35–42. [CrossRef]
47. Weiler, K.W.; Steenhuis, T.S.; Boll, J.; Kung, K.J.S. Comparison of Ground Penetrating Radar and Time-Domain Reflectometry as Soil Water Sensors. *Soil Sci. Soc. Am. J.* **1998**, *62*, 1237–1239. [CrossRef]
48. Leoni, A.; Mondot, M.; Durier, F.; Revellin, R.; Haberschill, P. Frost Formation and Development on Flat Plate: Experimental Investigation and Comparison to Predictive Methods. *Exp. Therm. Fluid Sci.* **2017**, *88*, 220–233. [CrossRef]